FRACTOGRAPHIC ASPECTS OF AL-ALLOY / SiC$_p$ METAL MATRIX COMPOSITE SUBJECTED TO STATIC, DYNAMIC AND CYCLIC MECHANICAL LOADING

* Tarpani J. R., Maluf O., Oliveira J., Seraphim B. E. H.
University of São Paulo, Av. Trab. Sãocarlense, 400, São Carlos-SP, 13566-590, Brazil
* jrpan@sc.usp.br, maluf@sc.usp.br, oliveira@sc.usp.br, seraphim@sc.usp.br

Abstract. AA356 alloy/SiC$_p$ compocast billets were produced via Vortex-Stir Compocasting technique and machined testpieces were subjected to static flexural, Charpy impact and fatigue testing with subsequent fractographical evaluation of broken specimen halves. Experimental results showed that T6 tempering increased both flexural stiffness and ultimate strength by 20% as compared to the properties of non-aged composite. Increasing temperature was found to have a beneficial effect on the impact toughness of T6 heat-treated composite. However, flexural strength of AA356-T6 alloy was impaired by 20% due to SiC particulate blending, and fatigue life was 10 to 25% shorter due to thermal aging of the composite. Documented evidence via microfractographic analysis is provided to shed some light on controlling mechanisms of fracture.

Introduction

The Vortex-Stir Compocasting technique allows for simple, fast and cost-effective manufacturing of ceramic particulate-reinforced metal-matrix composites (MMC), with the mixture performed in semi-solid state [1,2]. MMC are attractive materials for automotive industry for application in powertrains, valves and pistons, cylinder blocks, steering columns, and brake discs and calipers due to their higher wear resistance, better lubrication characteristics, more efficient heat dissipation, higher modulus of elasticity, and up to 50% lower weight than conventional materials [3]. Limitations of the technique include low wettability of ceramic particles by the metal molten matrix, difficulty in achieving uniform distribution of reinforcing particles and relatively high porosity of the end product [4,5].

In this work, AA356 alloy/SiC compocast billets (weighing ~3 kg) with particle reinforcing phase content of 10% in volume were produced. Static flexural strength, Charpy impact toughness and flexural fatigue of the compocast AA356 alloy/SiC$_p$ material were characterized at ambient and out-of-ambient temperatures in both heat treated and non-heat treated conditions. Fracture surfaces of tested coupons were subsequently examined by scanning electron microscopy to correlate their main topological aspects with mechanical test results.

Materials and Methods

Composite. AA356 aluminum alloy (Al-7Si-0.3Mg) was chosen due to its good fluidity, high silicon content to remain in liquid state at low temperatures for long periods in contact with SiC without generating Al$_4$C$_3$ while exhibiting a relatively broad semi-solid state interval, and its adequate amount of magnesium to both assist wettability of ceramic particles by the molten metal and produce strengthening second phases in thermal aging [1].

Black SiC with particle sizes of 30 to 50 μm was oxidized at 800°C to both reduce the formation of mechanically brittle and harmful Al$_4$C$_3$ compound and improve wettability of the particles by the AA356 alloy through the generation of a SiO$_2$ layer. A semi-automated thermo-mechanical device for incorporating ceramic reinforcement particles into the metal in semi-solid state was designed, developed, fabricated and put into operation based on various current mechanical designs described in the literature [4-6], from which the most advantageous characteristics were extracted while avoiding their main inconveniences. Some of the composite billets were subjected to T6 temper in

order to take advantage of the best combination of mechanical, physical and chemical properties of cast AA356 alloys [7].

The AA356/SiC$_p$ composite microstructure is illustrated in Fig. 1, where strengthening particles are visible in regions of eutectic composition around globular crystals of aluminum-rich α-matrix. Average Brinell hardness of AA356-T6 alloy was 63 HB, while the AA356/SiC$_p$-T6 composite reached 87 HB, clearly indicating the powerful hardening effect of SiC blending.
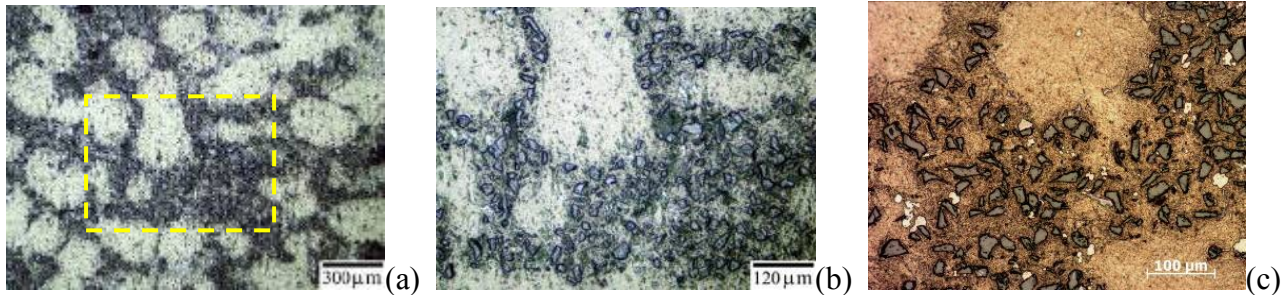

Fig. 1: (a) Micrographic features of metal-matrix compocast material; (b,c) Magnified views.

Monotonic Flexural. Three point-bend tests were carried out according to ASTM-C1421 standard devised to brittle materials. Type-A Charpy specimens containing electro-discharge machined straight notch with root radius of 100 μm were tested at ambient temperature at a load-line displacement rate of 0.5 mm/min. After reaching the ultimate load, test pieces collapsed catastrophically, determining the end-of-test condition. Testpiece stiffness, maximum load, maximum load toughness and maximum deflection were determined.

Charpy Toughness. Charpy impact toughness tests were conducted at 25°C and 300°C as per the ASTM-E23 standard, at an impact speed of 5.5 m/s in a fully instrumented 300 Joules capacity testing machine Specimens identical to those used in quasi-static flexure experiments were utilized. Absorbed impact energy was measured.

Fatigue. Three point-bend fatigue tests were performed in accordance with the ASTM-E466 standard, using identical specimens as described above. Constant stress-amplitude loading was applied at room temperature under a sinusoidal wave frequency of 10 Hz and a load ratio equal to 10. Maximum compressive loads varied from 10% to 60% of the rupture load determined in monotonic flexure tests, and the failure criterion adopted was complete rupture of the specimen. Stress-life (S-N) evaluation curves were developed.

Fractographic Inspection. Fracture surfaces of test coupons were examined fractographically by scanning electron microscopy (SEM) operating in secondary electron mode.

Results and Discussion
Mechanical Properties and Fractographic Analysis
Monotonic Flexural. Fig. 2 shows the results of monotonic flexure tests in terms of load vs. load-line deflection curves, from which the following conclusions can be drawn:
   (i)   T6 tempering increased stiffness and ultimate flexural strength of the MMC by 20%;
   (ii)   The stiffness of AA356-T6 alloy increased by 25% due to addition of SiC ceramic particles, but its capacity to withstand flexural loading was reduced by 20%.

According to Ref. 8, the relatively low fracture toughness is a property inherent to discontinuously particulate reinforced MMC and, disregarding intrinsic peculiarities of metallic alloys and casting processes, this low toughness originates from substantial differences between elastic, plastic and thermal properties of their metallic and ceramic constituents. These discrepancies degrade the metal matrix located at the vicinities of the metal/ceramic interface as a result of both the high strain-hardening capacity of the metal and stress intensification caused by the irregular and angular geometry of SiC particles. Thus, the metal matrix next to the interface is subject to highly localized damage leading to its premature fracture. The diagram in Fig. 2 shows the reduction on the capacity

of MMC to bend prior to fracture when compared to the Al-alloy from which it derives. Note also that although T6 tempering diminished the MMC ductility, the counterparting increase in fracture load more than compensated for this ductility loss, so that maximum load toughness (given by the product of maximum load vs. deflection) was favored by heat treatment. Both the stiffness increase and ductility loss were due to second phase precipitation during aging process, while the improvement in mechanical strength of the MMC may have occurred via relaxation of residual thermal and mechanical stresses (as pointed out by Ref. 8) during solution heat treatment of the material, owing basically to decreased yield strength of the metal matrix.
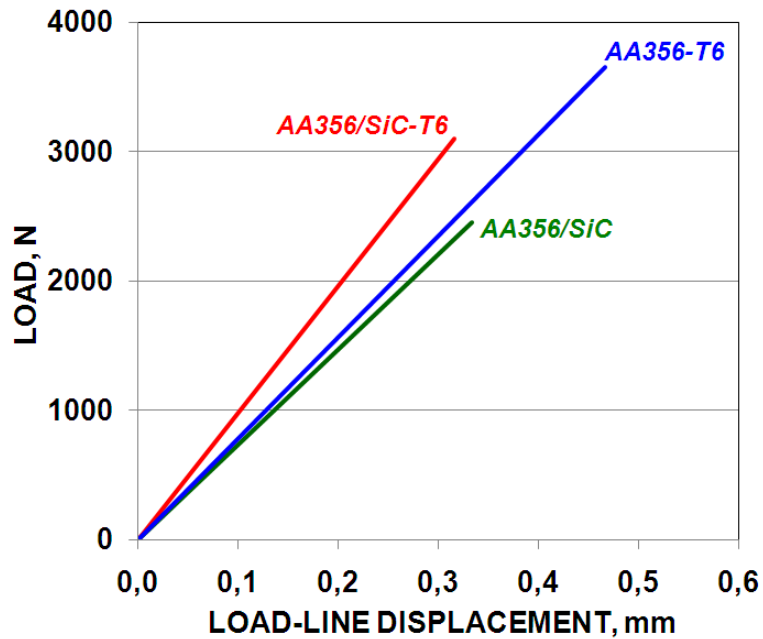

Fig. 2: Quasi-static flexure test results for AA356-T6 alloy and MMC with and without T6 heat treatment.

Fig. 3 shows SEM images of fracture surfaces created under quasi-static monotonic flexure of MMC with and without T6 heat treatment. Fractographic aspects of AA356-T6 alloy are also presented for deals of comparison.
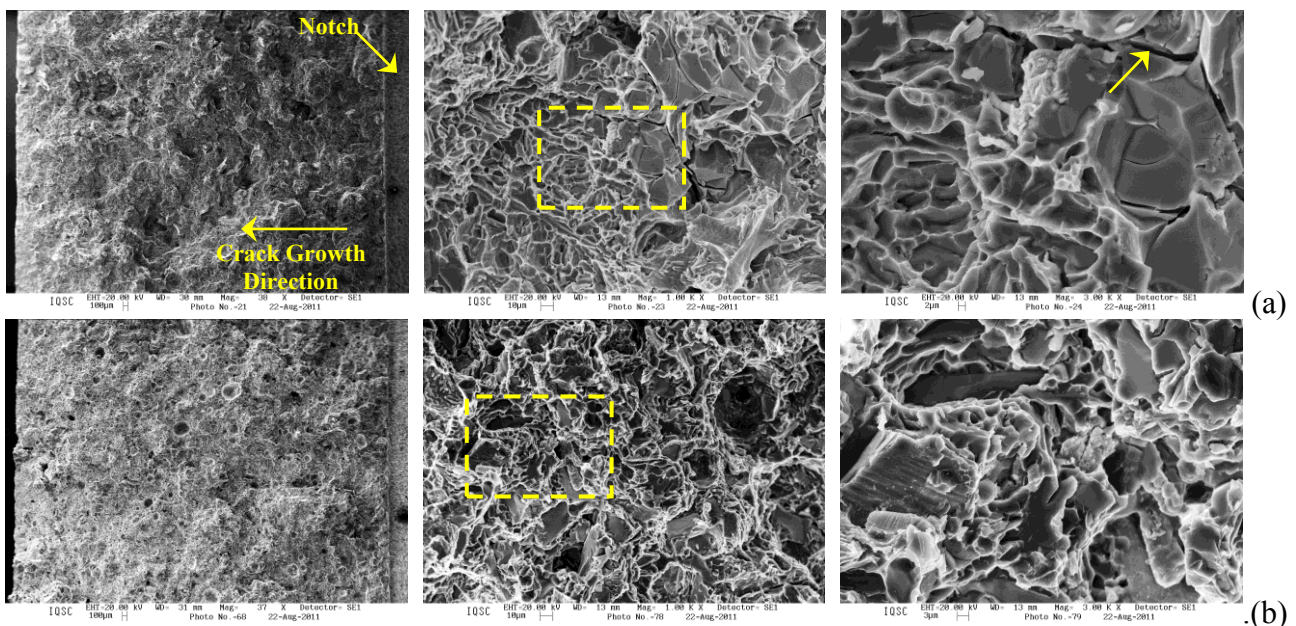

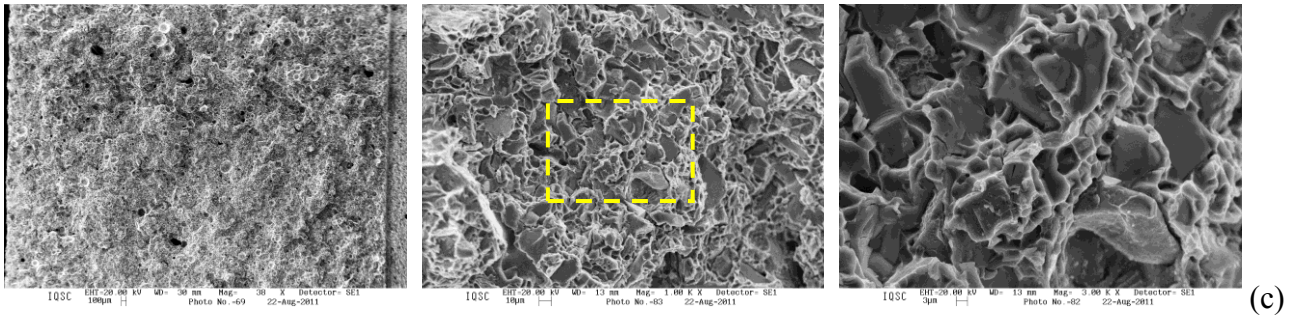*Fig. 3: Continued on the next page.*

Fig. 3: SEM images of fracture surfaces generated in quasi-static flexure tests: (a) AA356-T6 alloy; (b) Non-heat treated MMC; (c) MMC-T6.

Fig. 3a illustrates typical non-homogeneity of cast materials, in which areas of ductile fracture governed by void nucleation, growth and coalescence micromechanisms are mixed with areas of brittle fracture, where cracks (see arrow) follow low energy propagation paths. A comparison of Figs 3b and 3c, which correspond to the non-aged MMC and T6-treated MMC, respectively, confirms the greater ductility of non-heat treated matrix, as well as the higher tendency to fracture of reinforcing particles surrounded by aged metal matrix. This trend results from both the stiffer precipitate-containing matrix and stronger interaction between metallic and ceramic phases, as developed in T6 temper. The greater structural homogeneity of aged composite can also be inferred by comparing the above figures, and this was corroborated by the narrower-range experimental data scattering verified for the MMC-T6 as compared to non-heat treated material.

Charpy Toughness. Fig. 4 depicts Charpy impact results as a function of testing temperature, indicating that the AA356-T6 toughness is practically twice the corresponding MMC-T6. In both cases, temperature had a positive toughening effect on materials. However, stress concentration and intensification effects caused by sharp notching were particularly drastic for the MMC when compared to the original Al-alloy, insofar as the former material exhibited just a fraction of the neat alloy toughness. The deleteriousness of notching MMC specimens subjected to dynamic loading is undoubtedly the main restraining condition for a spreader use of this class of materials in high responsibility structural components, in which damage resistance and tolerance are *sine-qua-non* characteristics. In this regard, data points obtained in this study corroborated the well-established rule of greater severity of dynamic loads than quasi-static ones, since in the former loading mode time available for plastic deformation is short enough to suppress the development of this stress relief mechanism.
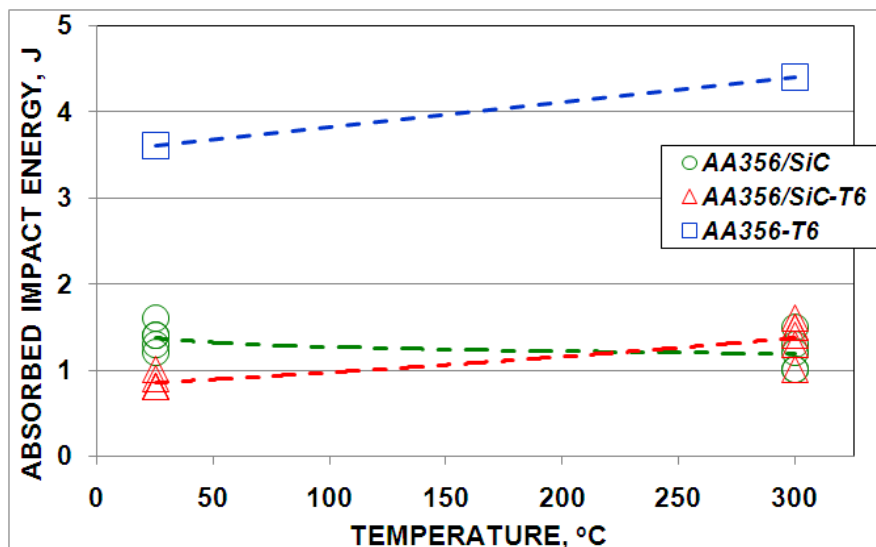

Fig. 4: Results of Charpy impact toughness tests of AA356-T6 alloy and MMC treated and non-heat treated to T6 temper.

Fig. 5 depicts fracture surfaces of test specimens subjected to impact at ambient temperature. Fig. 5a refers to AA356-T6 alloy, and corroborates previous observation in regard to structural non-homogeneity of cast materials, since areas of ductile and brittle fractures are interspersed. On the other hand, non-aged MMC (Fig. 5b) shows several SiC particles (indicated by arrows) at fracture surface, which is a clear indication of the embrittling effect of the ceramic phase. It is interesting to note that while slow flexural loading at room temperature seems to favor ductile fracture in non-heat-treated MMC (Fig. 3b), where nucleation, growth and coalescence of microvoids predominate and fracture occurs by particle debonding and pullout in MMC-T6 (Fig. 3c), the opposite behavior is observed under dynamic loading (Fig. 5). This may be due to the high susceptibility of aluminum alloys to strain-rate effects, as long as their fracture mechanisms are strain-controlled. T6 aging of MMC (Fig. 5c) appears not to favor material's dynamic toughness at 25°C (see Fig. 4) in the extensive presence of pores and clusters of SiC particles, since precipitation of second phases increases the matrix hardness considerably and thus limits the plasticity required to toughen the material [9].
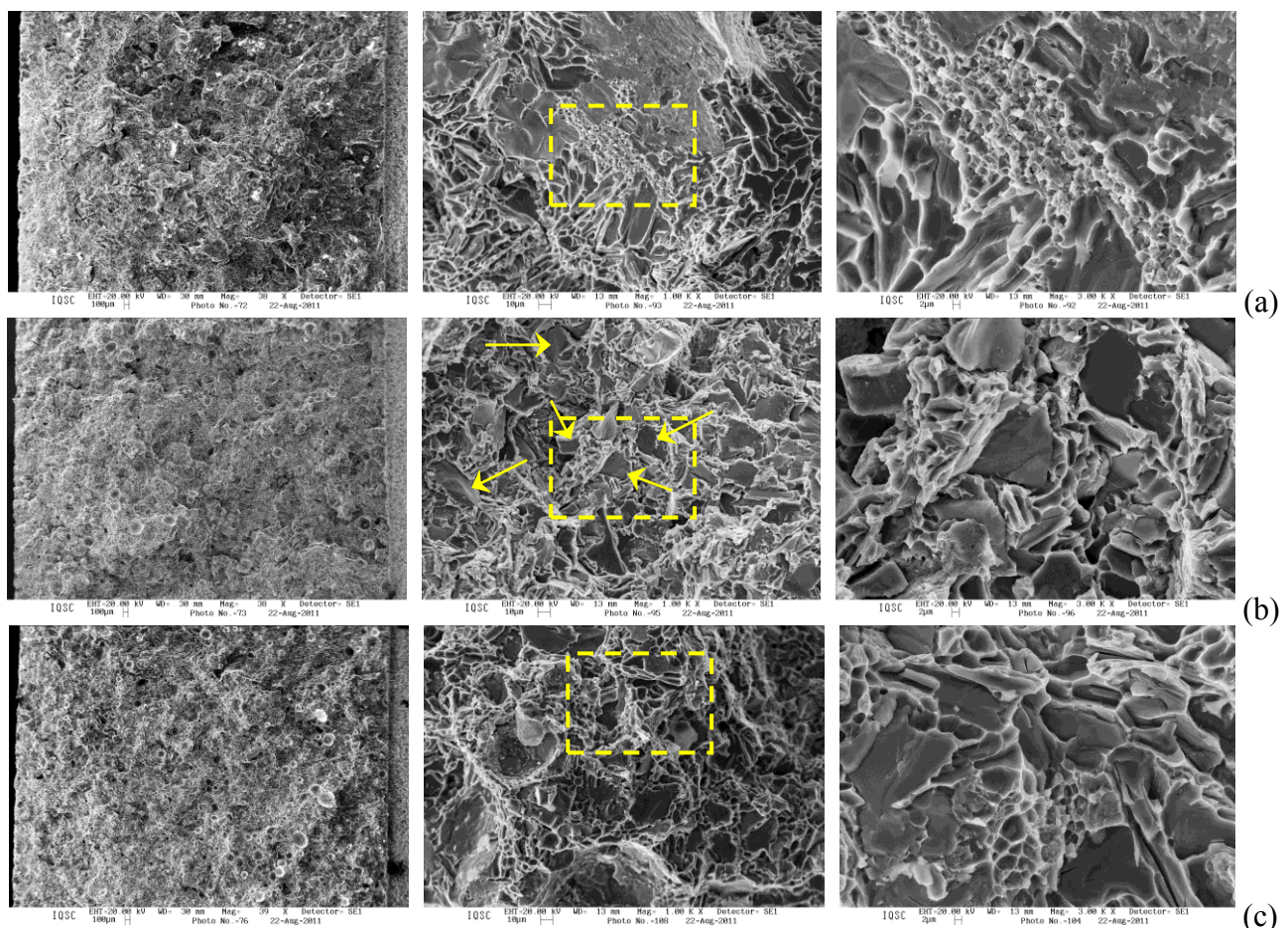

Fig. 5: Fractographic images of Charpy specimens impacted at room temperature: (a) AA356-T6 alloy; (b) Non-heat treated MMC; (c) MMC-T6.

Fig. 6 displays fracture surfaces of test specimens impacted at 300°C. Note the increase in area occupied by ductile fracture in the AA356-T6 alloy (Fig. 6a), which is consistent with the increase in absorbed energy shown in Fig. 4. For non-aged MMC (Fig. 6b), it can be inferred that the absence of an efficient interaction between metal matrix and ceramic particulate, allied to the decrease in hardening capacity of non-aged metallic-alloy at a relatively high temperature, are responsible for the drop in energy absorbed during impact (Fig. 4). In the case of MMC-T6 (Fig. 6c), there is clearly visible fracture of SiC particles (indicated by arrows), confirming a stronger adhesion between matrix and reinforcement phases. This feature, alongside the greater ductility of

metal matrix and the just slightly penalization of the alloy's yield strength and strain-hardening capacity at higher temperatures, due to matrix strengthening by precipitates from T6 temper [10], may have caused the small but consistent increase in Charpy toughness (Fig. 4).
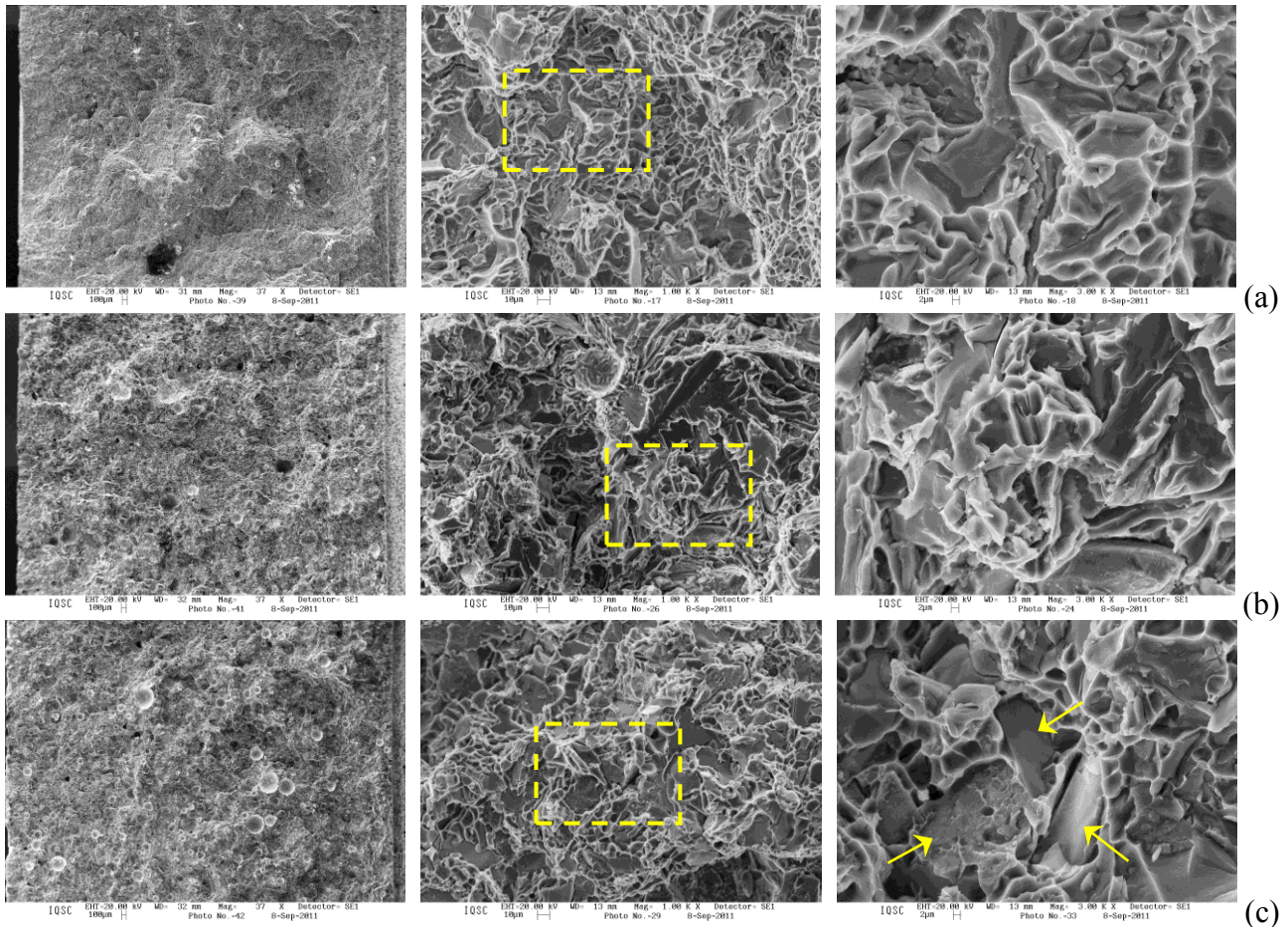

Fig. 6: SEM images of Charpy specimens impacted at 300°C: (a) AA356-T6 alloy; (b) Non-heat treated MMC; (c) MMC-T6.

Fatigue. Fig. 7 shows stress-life (S-N) curves obtained in flexural fatigue tests. Examining the curves at higher amplitude loads ($\geq$ 0.5 kN), i.e., for more critical fatigue loading condition, indicates that T6-treated and non-heat treated MMC present similar behaviors, an effect that is favored by the compressed scale of the graph. At lower amplitude loads (< 0.5 kN), a poorer behavior (shorter life) can be inferred for the heat-treated composite. However, this reduction in fatigue life can be considered modest, varying from 25% at intermediate levels of stress, to 10% at the lowest loading levels. According to Ref. 11, fatigue cracks in cast metal matrix composite reinforced with SiC particulate tend to propagate predominantly into the matrix phase, regardless of the applied stress level, avoiding ceramic particles due to their high mechanical strength and strong matrix/particle interface when good wettability of the particle system by molten metal is achieved in the composite manufacture stage. It is interesting to note that the only data point obtained for the AA356-T6 alloy does not differ significantly from the MMC behavior in both the conditions evaluated here.

Fig. 8 presents SEM microfractographs of fatigue fractured specimens. Documented evidence indicates that the ductility of AA356-T6 alloy suffices to generate perfectly visible fatigue striations (see arrow in Fig. 8a). On the other hand, in non-aged MMC (Fig. 8b), a profusion of SiC particles (indicated by arrows) appear on the fracture surface, supporting the hypothesis of low matrix/reinforcement interaction. This effect is less pronounced in Fig. 8c, conveying the assumption of improved adhesion between phases during T6 tempering. Lastly, in Fig. 8b, the

development of a degenerative striation pattern is clearly visible in non-aged MMC, while a toughening mechanism of fatigue crack deflection is visible in MMC-T6 shown in Fig. 8c.
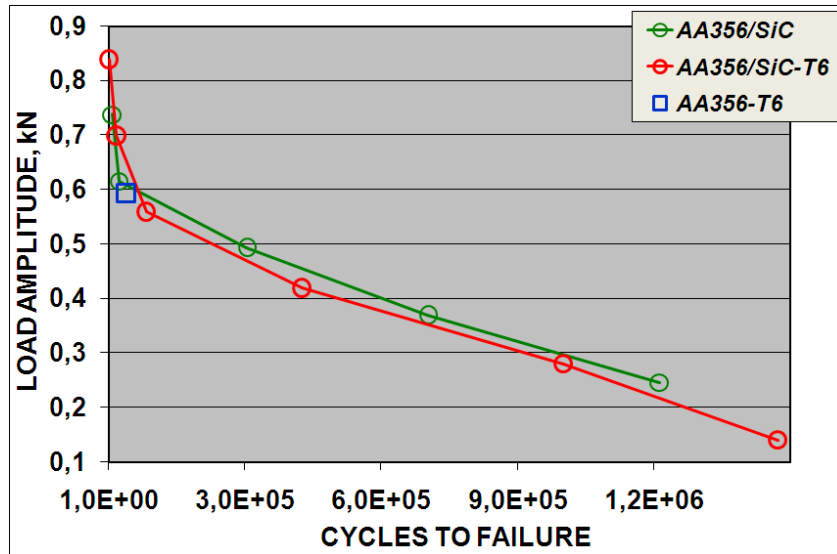

Fig. 7: Results of flexural fatigue tests of AA356-T6 alloy and MMC in T6-treated and non-heat treated conditions.
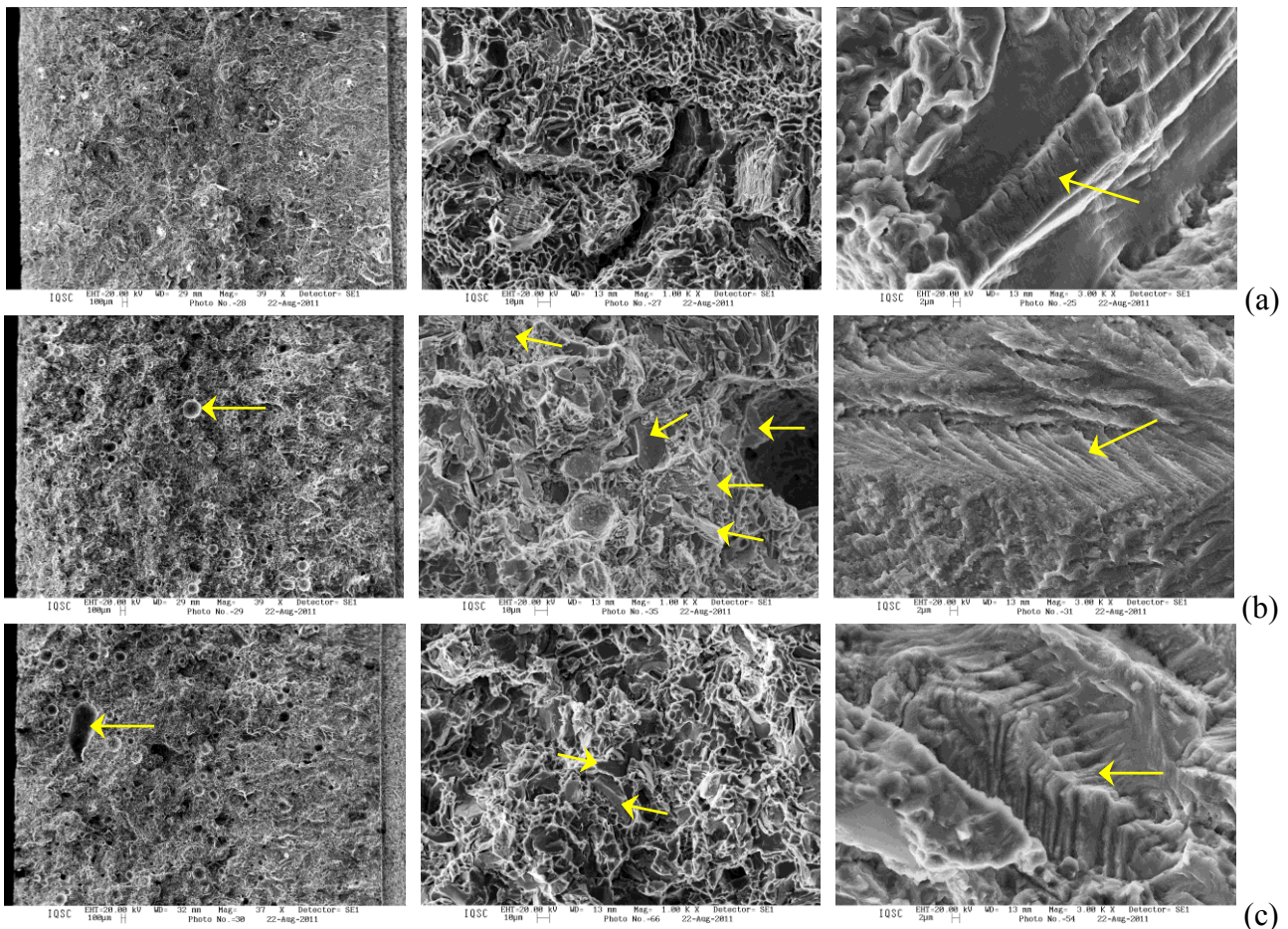

Fig. 8: SEM images of fracture surfaces generated by fatigue: (a) AA356-T6 alloy; (b) Non-heat treated MMC; (c) MMC-T6.

According to Ref. 12, porosity-type casting defects in AA359/SiC MMC appearing in fatigue fracture surfaces can reach a diameter of up to 700 µm, which is in very good agreement with the

pore arrowed in Fig. 8c. According to these authors, inclusion clusters sizing 100 μm in diameter are typical for the well-known Duralcan® industrial process, which is also in line with what can be observed in one of the microfractographs depicted in Fig. 8b.

Conclusions

1. Under quasi-static monotonic flexure at room temperature, MMC stiffness and ultimate strength showed a 20% increase due to T6 tempering. The increase in stiffness resulting from incorporation of SiC particles in AA356-T6 alloy was 25%, but it was offset by a 20% reduction in the corresponding fracture toughness;

2. Under Charpy impact, AA356-T6 alloy and MMC-T6 were toughened by increased testing temperatures. However, stress concentration and intensification caused by sharp notching was particularly drastic in the MMC case, so that its dynamic toughness was only a fraction of the AA356 alloy at the two evaluated temperatures;

3. Under flexural fatigue at room temperature there was no significant difference among S-N curves for the three studied materials, but at lower stress-amplitude levels, T6-treated MMC showed a distinctly visible tendency for shorter fatigue life than non-heat treated MMC;

4. All this evidence was documented through an extensive fractographic analysis.

References

[1] F. Akhlaghi, A. Lajevardi, H.M. Maghanaki: J. Mater. Process. Tech, Vol. 155&156 (2004) p.1874.

[2] W. Zhou, Z.M. Xu: J. Mater. Process. Tech. Vol. 63 (1997) p.358.

[3] N. Chawla, J.J. Williams, R. Saha: J. Light Metals Vol. 2 (2002) p.215.

[4] S. Balasivanandha, P.L. Karunamoorthy, S. Kathiresan, B. Mohan: J. Mater. Process. Tech. Vol. 171 (2006) p.268.

[5] S. Naher, D. Brabazon, L. Looney: J. Mater. Process. Tech. Vol. 166 (2004) p.430.

[6] M. Singla, D.D. Dwivedi, L. Singh, V. Chawla: J. Miner. & Mater. Charact. & Engng Vol. 8 (2009) p.455.

[7] Alcan Ingot Product Bulletin (2007) Alcan Prime Alloys – AA354, C355 & A356 Foundry Ingot, 16 p.

[8] M.M. Ranjbaran: Am. J. Sci. & Ind. Res. Vol. 1 (2010) p.549.

[9] I. Boromei, L. Cesquini, A, Morri, G.L. Garagnani, A. Maleque, R. Karim: Metal. Sci. & Tech. Vol. 24 (2009) p.12.

[10] V.S. Aigbodion, S.B. Hassan: J. Engng Res. Vol. 7 (2010) p.53.

[11] Z. Chen, P. He, L. Chen: J. Mater. Sci. & Tech. Vol. 23 (2007) p.213.

[12] P.K. Rohatgi, S. Alaraj, R.B. Thakkar, A. Daoud: Compos. A Vol. 38 (2007) p.1829.